CONFERENCE PRE-PRINT

DEVELOPMENT OF DATA ASSIMILATION SYSTEM ASTI TOWARD DIGITAL TWIN CONTROL OF FUSION PLASMA

Y. MORISHITA

Department of Nuclear Engineering, Kyoto University Kyoto, Japan

Email: morishita.yuya.7x@kyoto-u.ac.jp

S. MURAKAMI

Department of Nuclear Engineering, Kyoto University Kyoto, Japan

N. KENMOCHI

National Institute for Fusion Science, National Institutes of Natural Sciences Toki, Japan

H. FUNABA

National Institute for Fusion Science, National Institutes of Natural Sciences Toki, Japan

R. ICHIKAWA

Department of Nuclear Engineering, Kyoto University Kyoto, Japan

M. YOKOYAMA

National Institute for Fusion Science, National Institutes of Natural Sciences Rokkasho, Japan

G. UENO

The Institute of Statistical Mathematics, Research Organization of Information and Systems Tachikawa, Japan

M. OSAKABE

National Institute for Fusion Science, National Institutes of Natural Sciences Toki, Japan

Abstract

We have developed a model predictive control system for fusion plasmas based on data assimilation (DA), which integrates predictive model (digital twin) adaptation using real-time measurements and control estimation robust to model and observation uncertainties. The core part of the control system, ASTI (Assimilation System for Toroidal plasma Integrated simulation), predicts the probability distribution of future plasma states and estimates both the optimal control input and the actual plasma state based on Bayes' theorem. In this study, the ASTI-centered control system was implemented in the Large Helical Device (LHD) and successfully applied to control the plasma temperature and density. The control experiments demonstrate the effectiveness of the DA-based approach, which enables the synergistic interaction of measurement, heating, fueling, and simulation. This approach provides a flexible platform for digital twin control of future fusion reactors.

1. INTRODUCTION

The operation of future fusion reactors requires nonlinear and multivariate control of fusion plasma behavior under conditions of limited measurement. However, a predictive model (digital twin) essential for such complex control generally involves large uncertainties because it is inherently difficult to model all the components affecting the plasma behavior and their interactions with sufficient accuracy. To address this challenge, we are developing an analysis and control system, ASTI, based on a DA framework that integrates model adaptation and control estimation [1]. Typical DA is a statistical method to estimate the state vector, which consists of the variables in a numerical model, based on observation data and can make the behavior of the model similar to that of the real system. In addition to the state estimation, our innovative DA framework includes the estimation of control input

that leads the system state to the target state, which allows ASTI to achieve adaptive predictive control. The effectiveness of this control approach was demonstrated through a simple control experiment in LHD [2]. ASTI approximates the probability distribution of the state vector with a number of ensemble members (simulations with slightly different conditions) to realize its time evolution and the DA computation. ASTI can control both observable and unobservable variables and can be applied to complex control with multiple variables. In recent years, while research on machine learning-based control for individual control problems has advanced (e.g., [3]), studies on comprehensive control systems that harmoniously integrate numerous observations and actuators remain rather limited. The DA-based control provides a foundational framework for the harmonious overall control. In this approach, physics knowledge and control constraints can be easily incorporated into the control system through the state vector and the digital twin.

2. DATA ASSIMILATION-BASED CONTROL SYSTEM IN LHD

To investigate the control performance of ASTI for complicated control problems, we have built a control system based on ASTI at LHD [2,4]. We employ the integrated simulation code, TASK3D, as the digital twin of the LHD plasma in ASTI.

2.1. Data assimilation system ASTI

To extend the DA framework to an adaptive predictive control framework, we developed a new DA framework, DACS [1], which includes control processes. ASTI can realize adaptive model predictive control based on this DACS framework. Consider a control problem where the control estimation for the target state \mathbf{z} , and the measurement of the system state as \mathbf{y} are performed at every time interval Δt . We introduce the discrete time $\mathbf{t}_i = t_0 + i\Delta t$ ($i \in \mathbf{N}$), where t_0 is the initial time. The state vector at time t_i is defined as $\mathbf{x}_i = (\tilde{\mathbf{x}}_i, \mathbf{u}_i)$, where the vector $\tilde{\mathbf{x}}_i$ is the part of the state vector which contains the system state and the model parameters, and \mathbf{u}_i is the control input that affects the time evolution $\tilde{\mathbf{x}}_{i-1} \to \tilde{\mathbf{x}}_i$. The DACS framework assumes the state-space model:

$$\mathbf{x}_{i+1} = f_{i+1}(\mathbf{x}_i, \mathbf{v}_{i+1}),\tag{1}$$

$$\mathbf{z}_i = H_i^{\mathbf{z}} \mathbf{x}_i + \mathbf{w}_i^{\mathbf{z}}, \tag{2}$$

$$\mathbf{u}_i^* = H^{\mathbf{u}}\mathbf{x}_i + \mathbf{w}_i^{\mathbf{u}},\tag{3}$$

$$\mathbf{y}_i = H_i^{\mathbf{y}} \mathbf{x}_i + \mathbf{w}_i^{\mathbf{y}}. \tag{4}$$

The system model, Eq. (1), represents the time evolution of state vector \mathbf{x} from time t_i to t_{i+1} considering system noise \mathbf{v}_{i+1} . The operator f_{i+1} corresponds to the TASK3D simulation in this study. Equation (2) represents the relationship between \mathbf{x}_i and the target state \mathbf{z}_i using the matrix $H_i^{\mathbf{z}}$ and the associated noise $\mathbf{w}_i^{\mathbf{z}}$. In the same manner, Eqs. (3) and (4) represent the relationship between \mathbf{x}_i and the optimal control input \mathbf{u}_i^* and that between \mathbf{x}_i and the observation \mathbf{y}_i , respectively. In this study, each noise follows a Gaussian distribution, and the covariance matrices are key parameters of the control system that determine the control capability.

The state distribution $p(\mathbf{x})$ is represented by an ensemble $\{\mathbf{x}^{(k)}\}_{k=1}^n$, where k and n denote the ensemble index and the total number of ensemble members. The DACS framework has two major computational steps: prediction and filtering (assimilation). In the prediction step, each ensemble member evolves forward in time according to the system model (digital twin), producing an ensemble that approximates the state distribution at time $t+\Delta t$. The filtering step updates this distribution by incorporating information for system state estimation (adaptation) and control estimation. The resulting distribution $p(\mathbf{x}|\mathbf{d})$ reflects the assimilated information \mathbf{d} , where \mathbf{d} can be \mathbf{z} , \mathbf{u}^* , or \mathbf{y} . This assimilation process relies on Bayesian filters, such as the ensemble Kalman filter (EnKF) [5] and the particle filter [6], which impose (assimilate) the information (\mathbf{z} , \mathbf{u}^* , \mathbf{y}) using Eqs. (2-4).

Then, control estimation is performed by assimilating the target state \mathbf{z}_i into the distribution $p(\mathbf{x})$ to compute the z-filtered distribution $p(\mathbf{x}_i|\mathbf{z}_i)$. From this, the probability distribution of the control input required to achieve \mathbf{z}_i , $p(\mathbf{u}_i|\mathbf{z}_i)$, is obtained by marginalizing $p(\mathbf{x}_i|\mathbf{z}_i)$ with respect to $\tilde{\mathbf{x}}_i$. In this study, the optimal control input \mathbf{u}_i^* is defined as the expected value of \mathbf{u}_i under this distribution. The estimated control input is then incorporated into the predicted distribution through assimilation (u-filter) to compute the u-filtered distribution $p(\mathbf{x}_i|\mathbf{u}_i^*)$. This distribution represents the system state predicted when \mathbf{u}_i^* is applied. In addition, the system state including model parameters can be estimated by assimilating the observation \mathbf{y}_i into the latest distribution (y-filter).

2.2. TASK3D: Digital twin of the LHD plasma

In ASTI, we employ the integrated transport simulation code, TASK3D [7], as the digital twin for the LHD plasma. TASK3D solves the one-dimensional diffusive transport in the radial direction. In this study, assuming identical electron and ion density profiles, the particle transport equation,

$$\frac{\partial}{\partial t}(n\,\mathcal{V}') = -\frac{\partial}{\partial \rho}\mathcal{V}'\left\{\langle |\nabla \rho|\rangle n\,V - \langle |\nabla \rho|^2\rangle D\,\frac{\partial n}{\partial \rho}\right\} + S\mathcal{V}'$$

and the heat transport equations for the electron and ion species,

$$\frac{\partial}{\partial t} \left(\frac{3}{2} n \, T_s \mathcal{V}'^{5/3} \right) = -\mathcal{V}'^{2/3} \frac{\partial}{\partial \rho} \mathcal{V}' \left\{ \langle |\nabla \rho| \rangle \left(V_{K_S} + \frac{3}{2} V \right) n \, T_s - \langle |\nabla \rho|^2 \rangle \frac{3}{2} D \, T_s \frac{\partial n}{\partial \rho} - \langle |\nabla \rho|^2 \rangle n \, \chi_s \frac{\partial T_s}{\partial \rho} \right\} + P_s \mathcal{V}'^{5/3}$$

are solved. Here, n and T_s are the density and temperature of s-species. The parameter ρ is the normalized minor radius and $\langle \rangle$ represents the magnetic flux surface average. The term P_s is the heat source, \mathcal{V} is the plasma volume, and $\mathcal{V}' = d\mathcal{V}/d\rho$. The parameters V and V_{K_s} are the particle and heat pinch velocities, respectively, and are assumed to be determined by the neoclassical theory. In addition, D and χ_s are the particle and thermal diffusivities. As the diffusivity models, we employed the constant model for particle diffusivity and electron thermal diffusivity, and the gyro-Bohm model for ion thermal diffusivity.

Here, we use a typical magnetic configuration of LHD: the major radius of the magnetic axis at vacuum is 3.6 m and the magnetic field strength at the plasma centre is 2.85 T. The term P_s is determined by the ECH, NBI heating, and the power exchange between particle species. For real-time prediction for ECH, we employ the following simple model:

$$P_{\rm e}^{\rm ECH}(\rho) = \sum_{\xi} A_{\xi} \exp\left(-\frac{1}{2} \frac{\left(\mu_{\xi} - \rho\right)^2}{\sigma_{\xi}^2}\right),$$

where the profile parameter σ_{ξ} depends on the deposition position μ_{ξ} , and we estimated the value for each gyrotron ξ based on the detailed ray-tracing analysis (~0.015 for μ_{ξ} =0.1, ~0.03 for μ_{ξ} =0.4). The coefficient A is determined by the ECH input power. We assume that the ECH contributes directly only to the electron heat source term. For real-time computation of NBI heating, we employ the FIT3D-RC model [8]. This model calculates the NBI heat deposition and particle source profiles based on the surrogate model for fast ion birth and a simple analytical solution of the Fokker-Planck equation. The particle source S is primarily determined by the ionization of neutral particles. For the real-time computation of $\frac{1}{1}$ cap S, we also employed a surrogate model based on a neural network [4] for the AURORA model [9]. This surrogate model computes the particle source radial profile from the plasma temperature and density, and the neutral density at the plasma edge. We employ a simple gas-puff model where the neutral density is proportional to the applied voltage, which determines the frequency of the pulsed gas-puff. The TASK3D simulation using the surrogate models takes 0.13 seconds to perform the particle and heat transport calculation for one second.

2.3. Control system in LHD

We have built a control system based on ASTI at LHD, as shown in Fig.1. The NBI, ECH, and gas-puff systems are connected to ASTI as the actuators to control the plasma density and temperature. ASTI adjusts the on/off states of up to seven neutral beams, five gyrotrons, and the valve voltage of the gas puff every 0.3 seconds. The response of the LHD plasma is observed as the radial profiles of electron temperature and density by the real-time Thomson scattering measurement system [10,11], and the profiles are assimilated into the state distribution every 0.3 seconds. ASTI runs on a vector machine (128 parallel processes, maximum 384 ensemble members) or a part of Plasma Simulator RAIJIN (6144 parallel processes, maximum 12288 ensemble members). We have applied this control system to control problems such as radial profile control of electron temperature, simultaneous control of electron temperature and ion temperature.

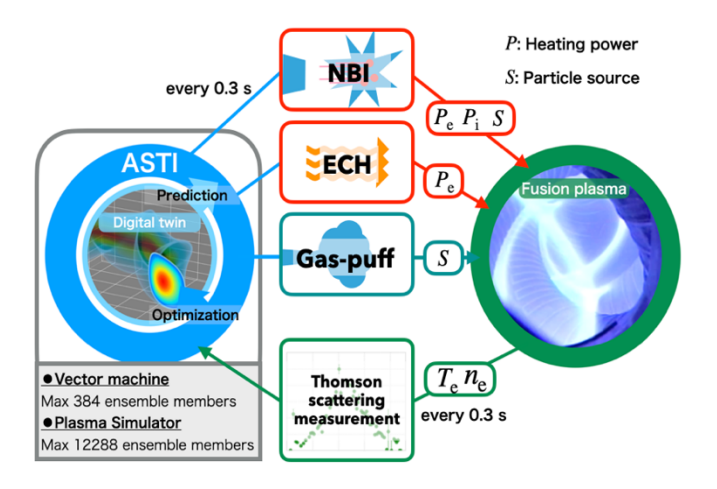


FIG. 1. Digital twin control system based on ASTI in LHD.

3. CONTROL EXPERIMENTS

Here, we present a demonstration experiment of simultaneous control of the electron temperature profile and central density. For this demonstration experiment, we used the ECH with two separate heating positions to control the radial profile of electron temperature. The two gyrotrons (total approximately 700 kW) are used for the heating at ρ =0, and the three gyrotrons (total approximately 1500 kW) are used for the heating at ρ =0.4. Each gyrotron can deliver three levels of power: zero (off), intermediate (e.g., half), and full, by utilizing modulation. For density control, ASTI adjusts the frequency of pulsed gas-puff with a width of 3 ms.

Table 1 lists the state variables, target variables, and observation variables for the experiment. Their radial profiles are defined on 11 grid points ($\rho = 0, 0.1, 0.2, \dots, 1$) in the state vector. The variables c_e , c_i , d, and v are introduced to optimize the transport parameters χ_e , χ_i , D, and V, respectively. In the prediction step, TASK3D computes the time evolution of the ensemble members by using $c_e\chi_e$, $c_i\chi_i$, dD, and V + v. Assimilation of the radial profiles of the electron density and temperature by the y-filter is expected to reduce the uncertainty in the transport parameters and improve the prediction performance.

TABLE 1. State variables, target variables, observation variables, and their dimensions (M_i). Standard deviations of the initial distribution (σ_{init}) and system noise (σ_{sys}) are also shown. The values with % as the unit represent the rate for determining the standard deviation in proportion to the state distribution mean.

	Variable		M_i	$\sigma_{ m init}$	$\sigma_{ m sys}$
x	n	Density	11	15%	5%
	$T_{ m e}$	Electron temperature	11	15%	5%
	$T_{ m i}$	Ion temperature	11	15%	5%
	$c_{ m e}$	Factor for electron thermal diffusivity	11	0.1	0.1
	c_{i}	Factor for ion thermal diffusivity	11	0.1	0.1
	d	Factor for particle diffusivity	11	0.1	0.1
	v	Additional convective velocity	10	0.1 m/s	0.1 m/s
	g	Factor for the coefficient in the gas-puff model	1	0.1	0.1
u	$P_{ECH}^{\rho=0}$, $P_{ECH}^{\rho=0.4}$	ECH input power for $\rho = 0 \& 0.4$	2	0	0.3 MW
	V	Voltage for the pulsed gas-puff	1	0	0.3 V
z	$T_{\rm e}^{ ho=0.1}, T_{\rm e}^{ ho=0.3}$	Electron temperature at $\rho = 0.1 \& 0.3$	2	•	•
	$n^{ ho=0.3}$	Density at $\rho = 0.3$	1		
у	n	Density	11		
	$T_{\mathbf{e}}$	Electron temperature	11		

ASTI computes 256 ensemble members (TASK3D simulations) in real time on a cluster PC with 128 parallel processes (vector computer). All filters are implemented by the EnKF. To avoid control instability in the initial phase, the behavior of the system model must be as close as possible to that of the real system before control begins. Thus, during the first phase t < 2.1 s, the plasma is heated by the fixed power $(P_{ECH}^{\rho=0}, P_{ECH}^{\rho=0.4}, V_{GP}) = (337 \text{ kW}, 389 \text{ kW}, 2 \text{ V})$, and ASTI only assimilates the observations to optimize the simulation model. ASTI starts to control the actuators from 2.1 s to produce a target state. The initial state distribution and system noise setting are shown in Table 1. We set the standard deviation of the target state noise to be 10 % of the target values. The variance of the control input noise can be set sufficiently small within the range that ensures stable data assimilation. We set the standard deviations to be 0.03 MW for P_{ECH} and 0.05 for V_{GP} . The standard deviation of the observation noise is assumed to be proportional to the difference between the observation and mean of the state distribution, $\sigma_y^l = r_y (y - H^y \hat{x})_l$, where σ_y^l is the standard deviation on the observation noise for the l-the element of y. The vector \hat{x} is the mean of the predicted distribution, and the subscript () $_l$ denotes the l-th element of the vector. In this experiment, we set the parameter r_y to be 0.8 [4].

We show the experimental results for the target $(T_{\rm e}^{\rho=0.1}, T_{\rm e}^{\rho=0.3}, n^{\rho=0.3}) = (2.5 \, {\rm keV}, 2 \, {\rm keV}, 2 \times 10^{19} \, {\rm m}^{-3})$. Figure 2 (a) shows the control result of electron temperature at the plasma center and (b) shows the result of electron density at $\rho=0.3$. We can see that both the electron temperature and density approach the target state at 3.5 s. ASTI has successfully adjusted the actuators as shown in Figs. 2(c) and (d). The control begins at 2.1 s, but it takes more than one second for the plasma state to reach the target state. This speed is strongly influenced by the magnitude of the target state noise and the uncertainty in the predicted distribution. If the target noise is set too small, the plasma state attempts to reach the target state quickly; however, since the EnKF is based on a kind of linear approximation, such aggressive control may lead to instability. Figures 2(e) and (f) show the radial profiles of the electron temperature and density. Both electron temperature and density are controlled and meet the conditions of the target state within 10 % error.

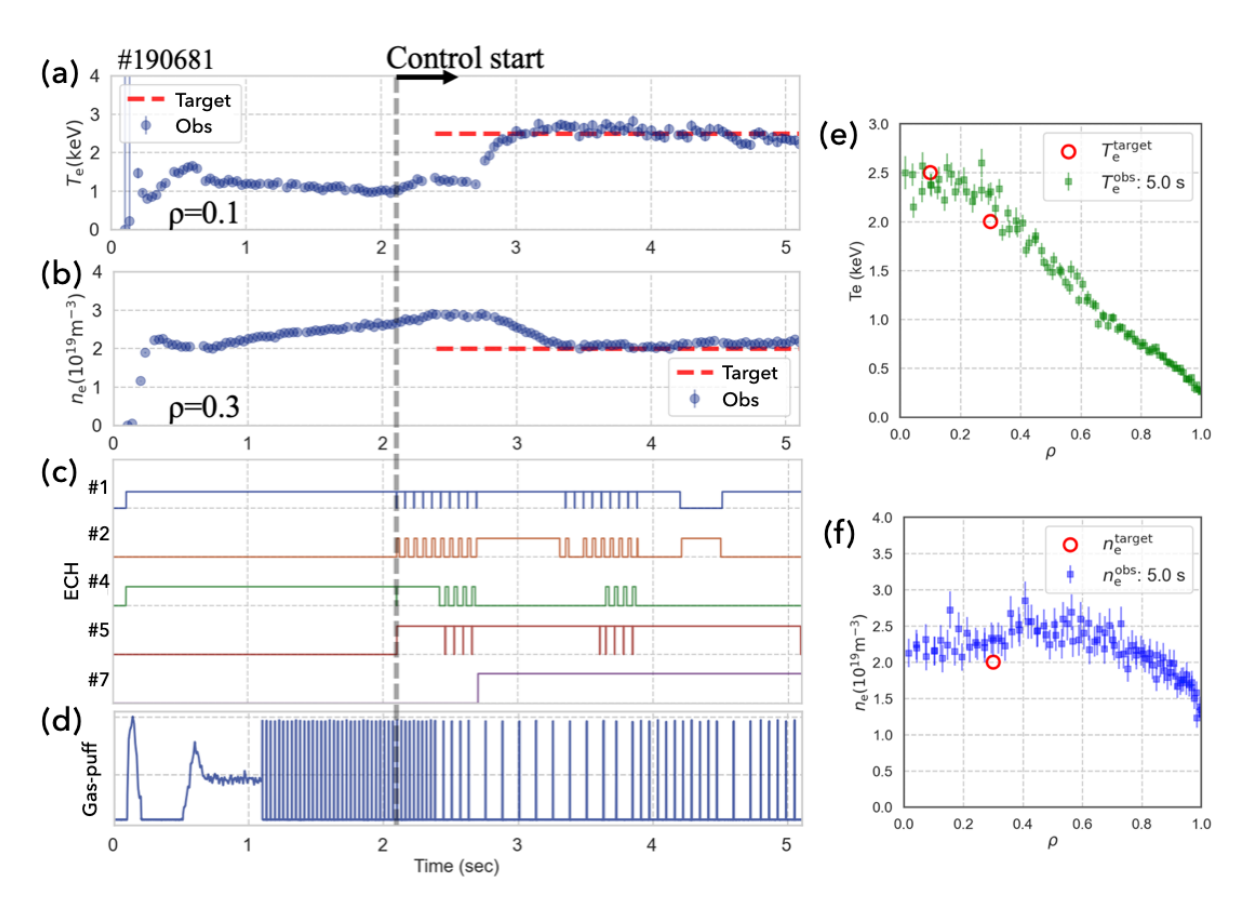


FIG.2. Results of an experiment to control the electron temperature and density (shot number: 190681). (a) and (b) Control results of electron temperature (center) and density ($\rho = 0.3$). (c) Adjusted input (on/off) to the ECH: #1, 2 for $\rho = 0$ and #4,5,7 for $\rho = 0.4$. (d) Waveform of the valve actuation voltage in the gaspuff. (e) and (f) Radial profiles of electron temperature and density at 5 s.

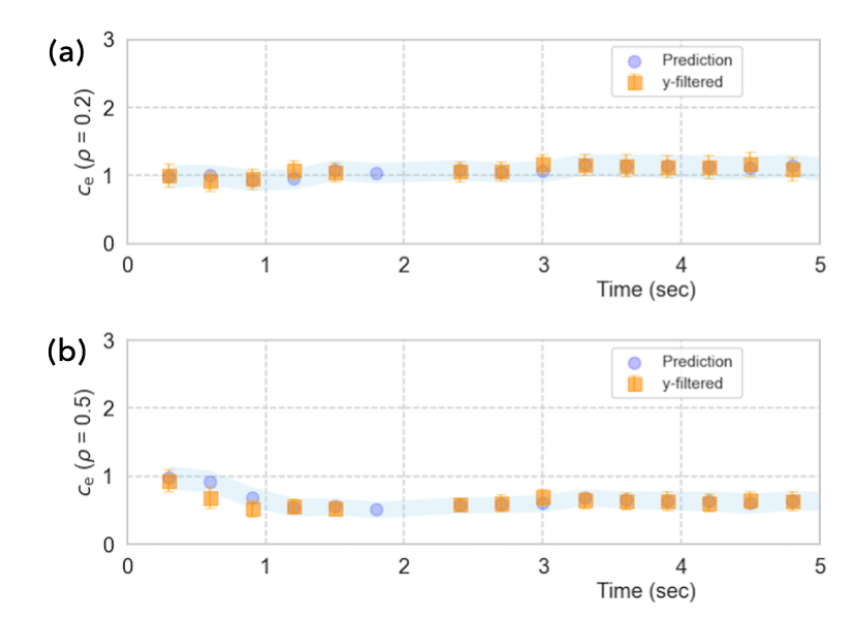


FIG.3. Time evolution of the estimated c_e at $\rho=0.3$ (a) and at $\rho=0.5$ (b). The hatching areas represent one standard deviation of the state distribution.

Figure 3 shows the time evolution of the factor for electron thermal diffusivity estimated based on the real-time observations. The factor for $\rho=0.5$ decreases to around 0.5 during the initial setup phase. However, even as the plasma state evolves thereafter, the value of the factor does not change significantly. This indicates that, although the electron thermal diffusivity has a spatial structure, it does not deviate substantially from the constant model and is sufficient for predicting electron temperature behavior of ECH-LHD plasma. This indicates that even a simple model can achieve effective control, as long as the actual plasma behavior falls within the expressible range of the model and the optimization using the real-time observations is sufficiently responsive.

We have also validated the effectiveness of this DA-based control approach in other control experiments including the simultaneous control of electron and ion temperatures, and have further confirmed the applicability of the particle filter within this control framework. While the particle filter entails substantial computational cost, it offers robust applicability to complex control problems, especially those with strong nonlinearities. We are preparing experiments where the ASTI system will operate on a supercomputer, "Plasma Simulator", located at Rokkasho, approximately 1,000 km away from the LHD, enabling remote control of the device. The communication link and control infrastructure have already been successfully established.

4. CONCLUSION

This study has demonstrated the effectiveness of the DA-based control using ASTI, which compensates for the digital twin imperfections using real-time observations and addresses complex multivariate control problems involving unobserved variables. This approach enables the construction of a comprehensive control system for fusion plasmas by synergistically integrating physical knowledge (including data-driven models), real-time observations, and actuators. ASTI can also contribute to control tasks that require the avoidance of terminating events by implementing relevant alarm rates and to physics experiments that require a high degree of control. Currently, ASTI is being extended for tokamak plasma control, and actual digital twin control experiments are planned. ASTI enables nonlinear and multivariate control of fusion plasma behavior under conditions of limited measurement and provides a foundation for flexible control of fusion reactors.

ACKNOWLEDGEMENTS

This work was supported by the NIFS Collaborative Research Program (NIFS22KAPT008 and NIFS23KIPT010), the ISM Cooperative Research Program (2022-ISMCRP-2026), JSPS KAKENHI (Grant Numbers JP23K19033, JP21K13901, and JP24K00609), and QST Research Collaboration for Fusion DEMO.

REFERENCES

- [1] MORISHITA Y. et al., Data assimilation and control system for adaptive model predictive control, J. Comput. Sci. **72** (2023) 102079.
- [2] MORISHITA Y. et al., First application of data assimilation-based control to fusion plasma, Sci. Rep. 14 (2024) 137.
- [3] SEO J. et al., Avoiding fusion plasma tearing instability with deep reinforcement learning, Nature 626 (2024) 746-751.
- [4] MORISHITA Y. et al., Development of Data Assimilation System for Temperature and Density Control in Helical Plasmas, Plasma and Fusion Res. **20** (2025) 1403034.
- [5] EVENSEN, G., The Ensemble Kalman Filter: theoretical formulation and practical implementation, Ocean Dynamics **53** (2003) 343-367.
- [6] KITAGAWA, G., Monte Carlo filter and smoother for non-Gaussian nonlinear state space models, Journal of computational and graphical statistics **5** (1996) 1-25.
- [7] MURAKAMI, S. *et al.*, Integrated simulation of high ion temperature plasmas of LHD, Plasma Phys. Control. Fusion **57** (2015) 119601.
- [8] MORISHITA Y. et al., Development of Rapid Simulation Code for NBI Heating Analysis in LHD, Journal of Fusion Energy 41 (2022) 1-8.
- [9] HUGHES M., A Monte Carlo algorithm for calculating neutral gas transport in cylindrical plasmas, Journal of Computational Physics **28** (1) (1978) 43–55.
- [10] FUNABA, H. *et al.*, Real-time electron temperature and density measurement by Thomson scattering for plasma control on LHD, 5th European Conference on Plasma Diagnostics (Proc. Int. Conf. Rethymno, Greece, 2023).
- [11] FUNABA, H. *et al.*, Electron temperature and density measurement by Thomson scattering with a high repetition rate laser of 20 kHz on LHD, Scientific Reports **12** (2022) 15112.